Power Electronics and Drives • AOP
Volume 4(39), 2019 DOI: 10.2478/pead-2019-0004

Power Electronics and Drives

Open-Phase Fault Detection Method for Sensorless Five-Phase Induction Motor Drives with an Inverter Output Filter

Research Article

Patryk Strankowski, Jarosław Guziński, Filip Wilczyński, Marcin Morawiec, Arkadiusz Lewicki

Gdańsk University of Technology- Faculty of Electrical and Control Engineering, G. Narutowicza 11/12, Gdańsk, Poland

Received July 31, 2018; Accepted January 18, 2019

Abstract: The paper presents the sensorless five-phase induction motor drive implementation with an inverter output filter with third harmonic injection. For the sensorless operation, the required observers are presented for the first and third harmonics with consideration of the inverter output filter. Moreover, the interaction of the observers and the control system is capable to handle a deactivation of one or two phases, which improves the reliability of the complete drive system. A new idea of online open-phase fault detection is presented based on the frequency analysis of the estimated observer variables. The test setup, fault operation capabilities and an experimental verification of the proposed fault detection method are presented in the paper.

Keywords: *Five-phase induction motor • Inverter output filter • Open-phase fault detection*

1. Introduction

Multiphase drives with a phase number higher than three are getting more and more interesting, where the number of publications related to this topic is growing. The most prominent representative is the five-phase drive system in which the focus is put on squirrel cage induction motors. These drive systems are known for the higher torque exploitation and overall higher reliability compared to the three-phase drive system. It might appear that the higher phase number leads to a higher cost of the drive. However, due to the current distribution into more phases, the rated phase current is in general lower than in the three-phase drive system of the same nominal power. For this reason, production cost of five-phase induction motor drives can be similar to the costs of a three-phase system. Nevertheless, the application of a more complex five-phase drive benefits from the overall reliability especially in the case of open-phase faults.

The authors in Wilczynski et al. (2017b) presented the potential of providing load torque, even if one or two stator phases are opened without changes in the control system. This indispensable advantage is especially important in drives with high reliability such as in the case of e-mobility, traction, aircraft actuators, elevators, ventilation and medical applications, where some of these areas are also known for providing relative long supply cables. In order to counteract this, different inverter output filters were designed to reduce the life shortening impact of the high dv/dt on the stator insulation and rotor bearings. However, the additional filter in the inverter output causes a voltage drop on the filter inductance that has to be considered especially in sensorless drive systems. In order to ensure a universal drive with high reliability, the paper presents the implementation of a sensorless five-phase induction motor drive with an inverter output filter and open-phase fault detection possibility.

* *E-mail: patryk.strankowski@pg.edu.pl, jaroslaw.guzinski@pg.edu.pl, fillip.wilczynski@pg.gda.pl, marcin.morawiec@pg.gda.pl, arkadiusz.lewicki@pg.edu.pl*

2. Five-phase induction motor drives with third harmonic injection

The possibility of providing a higher torque compared to three-phase induction motors is gained through the third harmonic injection in five-phase motor with concentrated windings. For this, the supply voltage is enhanced with a higher harmonic, which has adverse effects in three phase machines with further heating loses but can be utilised in five-phase machines (Levi, 2008; Levi et al., 2007). Furthermore, the third current harmonic injection results in a quasi-trapezoidal rotor flux distribution that in contrast to a sinusoidal flux distribution leads to better use of the stator magnetic circuit. The example of the resulting air gap flux distribution is presented in Fig. 1.

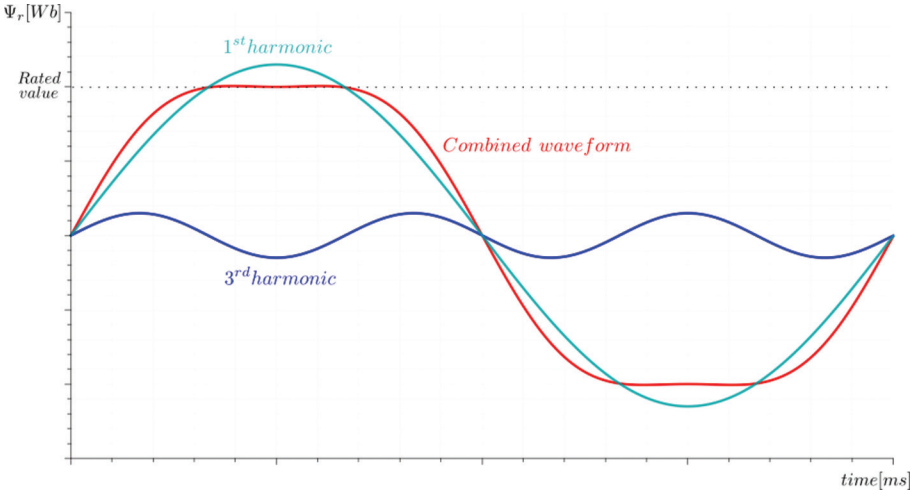

Fig. 1. Resulting rotor flux distribution for five-phase induction motor with third harmonic injection.

The summation of both flux components (Fig. 1) results in the required quasi-trapezoidal distribution. Nevertheless, both flux components have to be synchronised together to maintain the desired distribution (Guzinski et al., 2017a).

The Clarke transformation enables a conversion from five phases to two orthogonal frames (Ward and Härer, 1969) and is used to consider the five-phase machine as two independent machines in the first and the second orthogonal plane, which relates to first and third harmonic, respectively. The required transformation matrix for this consideration is denoted in Equation (1).

$$\begin{bmatrix} U_{\alpha 1} \\ U_{\beta 1} \\ U_{\alpha 3} \\ U_{\beta 3} \\ U_o \end{bmatrix} = \sqrt{\frac{2}{5}} \begin{bmatrix} 1 & \cos\left(\frac{2\pi}{5}\right) & \cos\left(\frac{4\pi}{5}\right) & \cos\left(\frac{4\pi}{5}\right) & \cos\left(\frac{2\pi}{5}\right) \\ 0 & \sin\left(\frac{2\pi}{5}\right) & \sin\left(\frac{4\pi}{5}\right) & -\sin\left(\frac{4\pi}{5}\right) & -\sin\left(\frac{2\pi}{5}\right) \\ 1 & \cos\left(\frac{4\pi}{5}\right) & \cos\left(\frac{8\pi}{5}\right) & \cos\left(\frac{8\pi}{5}\right) & \cos\left(\frac{4\pi}{5}\right) \\ 0 & \sin\left(\frac{4\pi}{5}\right) & \sin\left(\frac{8\pi}{5}\right) & -\sin\left(\frac{8\pi}{5}\right) & -\sin\left(\frac{4\pi}{5}\right) \\ \frac{1}{\sqrt{2}} & \frac{1}{\sqrt{2}} & \frac{1}{\sqrt{2}} & \frac{1}{\sqrt{2}} & \frac{1}{\sqrt{2}} \end{bmatrix} \cdot \begin{bmatrix} u_{a0} \\ u_{b0} \\ u_{c0} \\ u_{d0} \\ u_{e0} \end{bmatrix} \tag{1}$$

Therefore, the application of Equation (1) allows an independent consideration of both harmonics. As expected, in order to implement a sensorless drive system with the utilisation of the third harmonic, the voltage generation, the observer and the control system require a further second structure. The usage of an inverter output filter is here

as well processed as two separate elements in each orthogonal system and have to be considered in the control structure (Guzinski et al., 2015, 2017a).

The inverter output filter commonly used in the industry is the LC filter that acts as a low-pass filter and limits the impact of high dv/dt voltage increase that is generated through the pulse width modulation. The general structure of an LC filter is shown in Fig. 2, and for a detailed explanation about the element selection the reader is referred to the studies by Guzinski et al. (2015) and Guziński (2011).

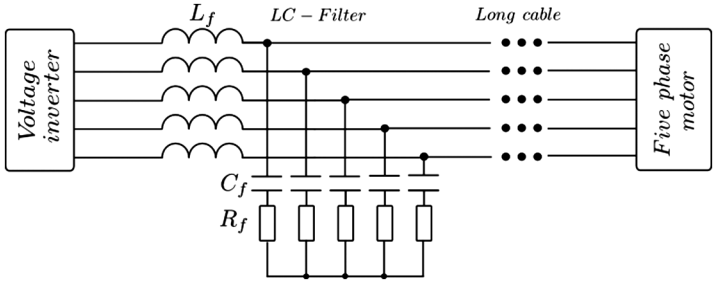

Fig. 2. LC filter structure in a five-phase drive system.

The positive effect to the motor stator voltage and current is presented in Fig. 3.

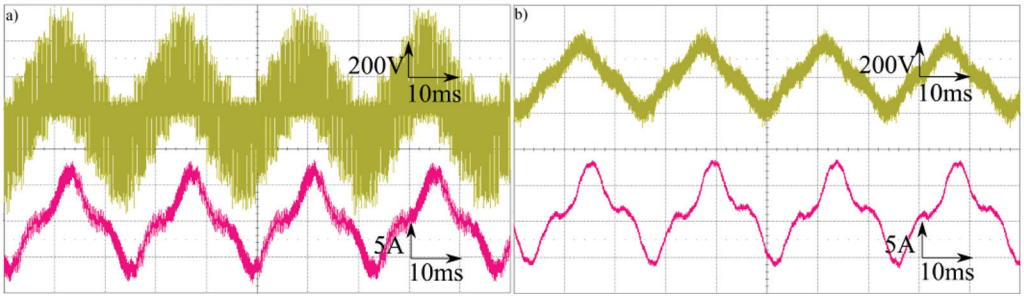

Fig. 3. Phase A current and voltage measurement at the inverter output (a) and at the motor input terminals (b) with third harmonic injection.

Fig. 3a illustrates the inverter output voltage and the filter input current in phase A, and Fig. 3b demonstrates the smoothed motor stator voltage and current. Both oscillograms present the motor operation with third harmonic injection under loaded drive conditions.

The benefits gained through the LC filter integration are decreased parasitic current flow through motor bearings, reduced stress on stator winding insulation, lower electromagnetic disturbances and so on. Nevertheless, the usage of an LC filter requires the consideration in the control structure and observer in both orthogonal frames (Guzinski et al., 2017a).

3. Sensorless control based on multiscalar variables with third harmonic injection

There are several control systems that were implemented in connection with five-phase induction motors, i.e., field-oriented control (Wilczynski et al., 2017a), direct torque control (Payami and Behera, 2017) and multiscalar model based (Adamowicz et al., 2015, 2016). In order to benefit from the third harmonic injection, two independent control systems for every orthogonal plane have to be implemented. However, the dedicated control systems have to handle the synchronisation difficulty of both rotor flux components. The proposed control, which is presented in the paper, is based on multiscalar variables that allow an independent control of the rotor flux and electromotive force and was presented in the studies by Guzinski et al. (2017a), Adamowicz et al. (2016) and Strankowski et al. (2017).

The controlled multiscalar variables are described as follows:

$$x_{11}^{(I)} = \omega_r^{(I)} \tag{2}$$

$$x_{12}^{(i)} = \psi_{r\alpha}^{(i)} i_{s\beta}^{(i)} - \psi_{r\beta}^{(i)} i_{s\alpha}^{(i)} \tag{3}$$

$$x_{21}^{(i)} = \psi_{r\alpha}^{2(i)} + \psi_{r\beta}^{2(i)} \tag{4}$$

$$x_{22}^{(i)} = \psi_{r\alpha}^{(i)} i_{s\alpha}^{(i)} + \psi_{r\beta}^{(i)} i_{s\beta}^{(i)} \tag{5}$$

where x_{11} is the rotor angular speed, x_{12} is proportional to the electromotive force, x_{21} is the square of the rotor flux vector products and x_{22} is the scalar product of the stator current and rotor flux. The index *(i)* describes the applied orthogonal plane for the first and third harmonics.

Fig. 4 demonstrates the control system structure with rotor flux synchronisation.

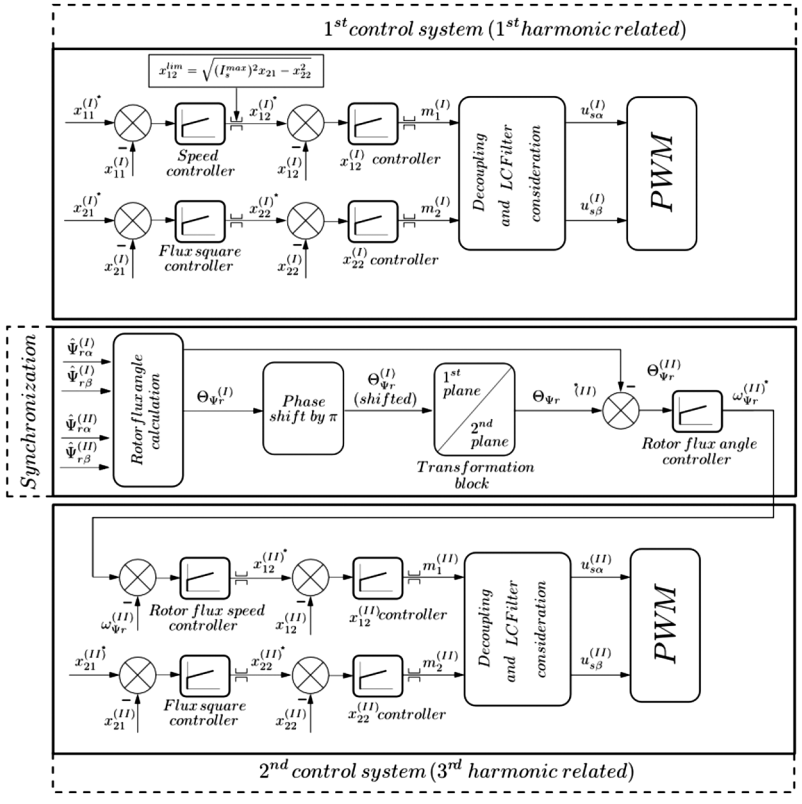

Fig. 4. Multiscalar control system structure for a five-phase induction motor with third harmonic injection and flux synchronisation.

As can be seen in Fig. 4, the variable x_{21}, that is responsible for the rotor flux, can be controlled independently from the first control structure, which is indispensable for utilising the third harmonic. The rotor flux angle of both systems is calculated based on the observed variables and is used for the rotor flux synchronisation procedure. The LC filter consideration is performed as presented in the studies by Guzinski et al. (2015) and Guziński (2011). The synchronisation procedure and thereby the resulting rotor flux distribution and rotor speed estimation error before and after the synchronisation are presented in Fig. 5.

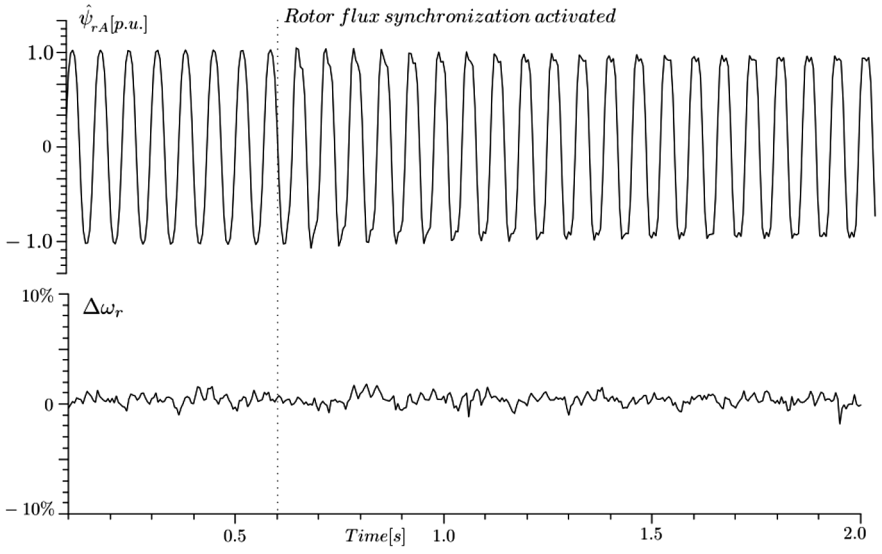

Fig. 5. Estimated rotor flux in phase A and speed estimation error while synchronisation procedure.

As can be seen in Fig. 5, the exemplary flux synchronisation is executed during the drive operation with first harmonic only. After the third harmonic voltage addition, both fluxes are synchronised together. The speed estimation error $\Delta\omega_r = \widehat{\omega_r} - \omega_r$ holds steady value of about 1% during the synchronisation process.

It is obvious that the voltage generation requires also an independent generation of both voltage components. For a detailed explanation about the PWM (Pulse Width Modulation) implementation, the reader is referred to the studies by Lewicki et al. (2016a, 2016b, 2017a, 2017b, 2017c).

The total harmonic distortion (THD) of the inverter output filter current for different loads is calculated as presented in Equation (6). In contrast to regular THD calculations in three-phase drives, the third harmonic has to be involved in the fundamental harmonic.

$$\text{THD}\ (\%) = \frac{\sqrt{\sum_{n=2,4,5,6,\ldots}^{50} I_n^2}}{\sqrt{I_1^2 + I_3^2}} \times 100 \tag{6}$$

where I_n is the current harmonic and n is the harmonic number.

Table 1. Parameters of the five-phase induction motor and LC filter

No load	Half nominal load	Nominal load
5.33%	1.37%	0.73%

As expected, the sensorless configuration of such a control system requires the implementation of two separate observers, each for the first and second control systems. Both observers have to consider the presence of the LC filter to calculate the actual stator voltage of the motor. The presented observer for the first plane estimates the rotor speed Equation (17) based on the estimation of the stator current, rotor flux, electromotive force, capacitor voltage drop and inverter output current (Equations (7–16)), where the stator current estimation includes the stator voltage calculation through the capacitor voltage estimation and was generally presented in the studies by Guzinski et al. (2015, 2017a) and Guzinski (2009). The first plane observer is denoted in Equations (7–17).

$$\frac{d\hat{i}_{s\alpha}}{d\tau} = a_1 \cdot \hat{i}_{s\alpha} + a_2 \cdot \hat{\psi}_{r\alpha} + a_3 \cdot \hat{\zeta}_{\beta} + a_4 \cdot (\hat{u}_{c\alpha} + (\hat{i}_{1\alpha} - \hat{i}_{s\alpha})R_f) + k_1 \cdot (\hat{i}_{1\alpha} - i_{1\alpha}) \tag{7}$$

$$\frac{d\hat{i}_{s\beta}}{d\tau} = a_1 \cdot \hat{i}_{s\beta} + a_2 \cdot \hat{\psi}_{r\beta} - a_3 \cdot \hat{\zeta}_{\alpha} + a_4 \cdot (\hat{u}_{c\beta} + (\hat{i}_{1\beta} - \hat{i}_{s\beta})R_f) + k_1 \cdot (\hat{i}_{1\beta} - i_{1\beta}) \tag{8}$$

$$\frac{d\hat{\psi}_{r\alpha}}{d\tau} = a_5 \cdot \hat{\psi}_{r\alpha} + a_6 \cdot \hat{i}_{s\alpha} - \hat{\zeta}_{\beta} + k_2 \cdot (\hat{\zeta}_{\beta} - \hat{\omega}_r \cdot \hat{\psi}_{r\beta})) \tag{9}$$

$$\frac{d\hat{\psi}_{r\beta}}{d\tau} = a_5 \cdot \hat{\psi}_{r\beta} + a_6 \cdot \hat{i}_{s\beta} + \hat{\zeta}_{\alpha} - k_2 \cdot (\hat{\zeta}_{\alpha} - \hat{\omega}_r \cdot \hat{\psi}_{r\alpha})) \tag{10}$$

$$\frac{d\hat{\zeta}_{\alpha}}{d\tau} = a_5 \cdot \hat{\zeta}_{\alpha} - \hat{\omega}_r \cdot \hat{\zeta}_{\beta} - a_6 \cdot \hat{i}_{s\alpha} + k_3 \cdot (\hat{i}_{1\alpha} - i_{1\alpha}) \tag{11}$$

$$\frac{d\hat{\zeta}_{\beta}}{d\tau} = a_5 \cdot \hat{\zeta}_{\beta} + \hat{\omega}_r \cdot \hat{\zeta}_{\alpha} - a_6 \cdot \hat{i}_{s\beta} + k_3 \cdot (\hat{i}_{1\beta} - i_{1\beta}) \tag{12}$$

$$\frac{d\hat{u}_{c\alpha}}{d\tau} = \frac{(\hat{i}_{1\alpha} - \hat{i}_{s\alpha})}{C_f} - \hat{u}_{c\alpha} \tag{13}$$

$$\frac{d\hat{u}_{c\beta}}{d\tau} = \frac{(\hat{i}_{1\beta} - \hat{i}_{s\beta})}{C_f} - \hat{u}_{c\beta} \tag{14}$$

$$\frac{d\hat{i}_{1\alpha}}{d\tau} = \left(\frac{u^*_{s\alpha} - R_f \cdot \hat{i}_{1\alpha} - R_f \cdot (\hat{i}_{1\alpha} - \hat{i}_{s\alpha}) - \hat{u}_{c\alpha}}{L_f} \right) + k_5 \cdot (\hat{i}_{1\alpha} - i_{1\alpha}) + k_6 \cdot (\hat{i}_{1\beta} - i_{1\beta}) \tag{15}$$

$$\frac{d\hat{i}_{1\beta}}{d\tau} = \left(\frac{u^*_{s\beta} - R_f \cdot \hat{i}_{1\beta} - R_f \cdot (\hat{i}_{1\beta} - \hat{i}_{s\beta}) - \hat{u}_{c\beta}}{L_f} \right) + k_5 \cdot (\hat{i}_{1\beta} - i_{1\beta}) - k_6 \cdot (\hat{i}_{1\alpha} - i_{1\alpha}) \tag{16}$$

$$\hat{\omega}_r = \frac{\hat{\zeta}_{\alpha}\hat{\psi}_{r\alpha} + \hat{\zeta}_{\beta}\hat{\psi}_{r\beta}}{\hat{\psi}^2_{r\alpha} + \hat{\psi}^2_{r\beta}} \tag{17}$$

where $\hat{i}_s$ represents the motor stator current, $\hat{\psi}_r$ the rotor flux, $\hat{\zeta}$ the electromotive force, $\hat{u}_c$ the capacitor voltage, $\hat{i}_s$ the inverter output current and $\hat{\omega}_r$ the rotor speed. The hat operator indicates that the estimated variables, $k_1 \ldots k_6$, are the observer coefficients, R_f the filter resistance, L_f the filter inductance, C_f the filter capacitance and u_s the stator voltage. The coefficients $a_1 \ldots a_6$ are defined in relation to motor parameters as follows: $a_1 = -(R_s L_r^2 + R_r L_m^2) / L_r w_\sigma$, $a_2 = R_r L_m / L_r w_\sigma$, $a_3 = L_m / w_\sigma$, $a_4 = L_r / w_\sigma a_5 = R_r L_m / L_r$, $a_6 = -R_r / L_r$, $w_\sigma = L_r L_s - L_m^2$ and have to be calculated separately for the first and the second plane, for the reason that the five-phase induction motor parameters are different in each control plane (Levi, 2008; Levi et al., 2007).

The presented observer, general structure of which was presented in the study by Krzeminski (2000), was previously used for three-phase drives and provided an accurate estimation of the rotor speed (Guziński, 2008). The observer of the second plane was designed less complex for the reason that the rotor flux estimation is required only to synchronise flux component of the third harmonic. Nevertheless, this structure should also include the estimation of the stator current, capacitor voltage drop and the filter inductance current. The observer is based on the Luenberger observer with extension of the filter current and voltage consideration according to Equations (18–25):

$$\frac{d\hat{i}_{s\alpha}}{d\tau} = a_1 \cdot \hat{i}_{s\alpha} + a_2 \cdot \hat{\psi}_{r\alpha} - a_3 \cdot \hat{\psi}_{r\beta} \cdot 3\hat{\omega}_r + a_4 \cdot (\hat{u}_{c\alpha} + (\hat{i}_{1\alpha} - \hat{i}_{s\alpha})R_f) + k_1 \cdot (\hat{i}_{1\alpha} - i_{1\alpha}) \tag{18}$$

$$\frac{d\hat{i}_{s\beta}}{d\tau} = a_1 \cdot \hat{i}_{s\beta} + a_2 \cdot \hat{\psi}_{r\beta} + a_3 \cdot \hat{\psi}_{r\alpha} \cdot 3\hat{\omega}_r + a_4 \cdot (\hat{u}_{c\beta} + (\hat{i}_{1\beta} - \hat{i}_{s\beta})R_f) + k_1 \cdot (\hat{i}_{1\beta} - i_{1\beta}) \tag{19}$$

$$\frac{d\hat{\psi}_{r\alpha}}{d\tau} = a_5 \cdot \hat{\psi}_{r\alpha} + a_6 \cdot \hat{i}_{s\alpha} + 3\hat{\omega}_r \cdot \hat{\psi}_{r\beta} + k_2 \cdot (\hat{i}_{1\alpha} - i_{1\alpha}) + k_3 \cdot 3\hat{\omega}_r \cdot (\hat{i}_{1\alpha} - i_{1\alpha}) \tag{20}$$

$$\frac{d\hat{\psi}_{r\beta}}{d\tau} = a_5 \cdot \hat{\psi}_{r\beta} + a_6 \cdot \hat{i}_{s\beta} - 3\hat{\omega}_r \cdot \hat{\psi}_{r\alpha} + k_2 \cdot (\hat{i}_{1\beta} - i_{1\beta}) + k_3 \cdot 3\hat{\omega}_r \cdot (\hat{i}_{1\beta} - i_{1\beta}) \tag{21}$$

$$\frac{d\hat{u}_{c\alpha}}{d\tau} = \frac{(\hat{i}_{1\alpha} - i_{s\alpha})}{C_f} - \hat{u}_{1\alpha} \tag{22}$$

$$\frac{d\hat{u}_{c\beta}}{d\tau} = \frac{(\hat{i}_{1\beta} - i_{s\beta})}{C_f} - \hat{u}_{1\beta} \tag{23}$$

$$\frac{d\hat{i}_{1\alpha}}{d\tau} = \left(\frac{u^*_{s\alpha} - R_{ind} \cdot \hat{i}_{1\alpha} - R_f \cdot (\hat{i}_{1\alpha} - \hat{i}_{s\alpha}) - \hat{u}_{c\alpha}}{L_f} \right) + k_5 \cdot (\hat{i}_{1\alpha} - i_{1\alpha}) \tag{24}$$

$$\frac{d\hat{i}_{1\beta}}{d\tau} = \left(\frac{u^*_{s\beta} - R_{ind} \cdot \hat{i}_{1\beta} - R_f \cdot (\hat{i}_{1\beta} - \hat{i}_{s\beta}) - \hat{u}_{c\beta}}{L_f} \right) + k_5 \cdot (\hat{i}_{1\alpha} - i_{1\beta}) \tag{25}$$

The variable notation is according to the first plane observer, however, considered as a separate drive system. Both observers ensure a good cooperation of the control systems and are used for further fault detection procedure as well.

4. Open-phase fault detection

The following section is dedicated to the sensorless open-phase fault detection of the experimental drive system. The test setup parameters are shown in Table 2, whereas the structure is illustrated in Fig. 6.

Table 2. Parameters of the five-phase drive system

Rated output power	5.5 kW
Rated current	8.8 A
Rated phase voltage	173 V
Number of poles	4
Rated torque	36.5 Nm
Rated speed	1440 rpm
Filter inductance	5 mH
Filter capacitance	14 µF
Filter resistance	1.1 Ω
Transistor switching frequency	3.3 kHz

The open-phase fault generation (Fig. 6) is done through conventional circuit breakers that are manually switched. The measurements are located inside the voltage inverter and include the DC-link voltage and four inverter output phase currents, which are required for the sensorless control. The fifth phase current is calculated with the help of Kirchhoff's Current Law (KCL).

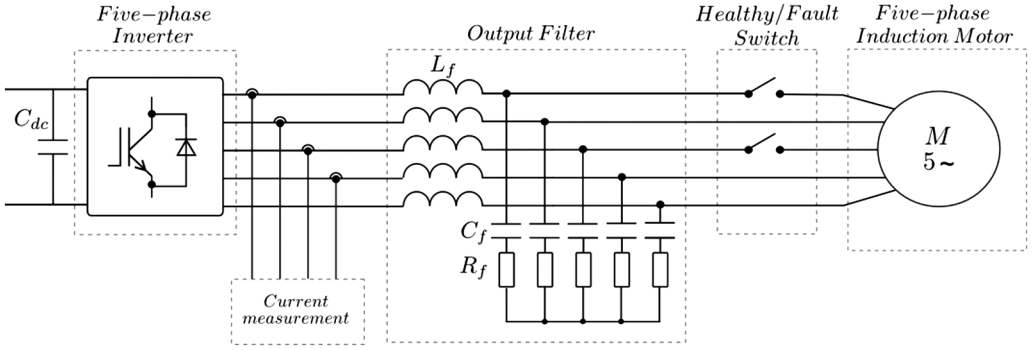

Fig. 6. Open-phase test setup for sensorless five-phase induction motor drive with an inverter output filter.

The first experiment (Fig. 7) illustrates the open-phase operation capabilities of the five-phase induction motor system. It has to be mentioned here that a non-critical operation with two opened phases is possible, if the non-adjacent phases are opened, i.e., A–C, B–D, C–E etc., as presented in the studies by Guzinski et al. (2017b), and Wilczynski et al. (2017c).

Fig. 7 demonstrates the drive operation, while a successive phase deactivation of A and C under light load, i.e., T_{LOAD}= 0.3 p.u. The measured rotor speed ω_r, estimated rotor speed $\widehat{\omega}_r$ and the measured stator current vector magnitude i_m of all phases in the first plane are presented.

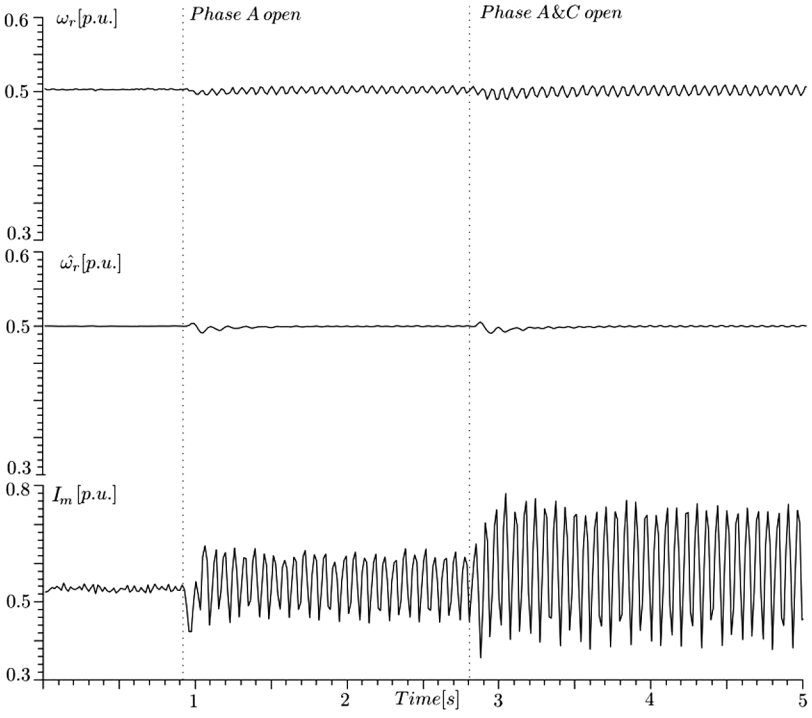

Fig. 7. Operation capabilities of the five-phase induction motor drive with one or two opened phases under light load T_{L}= 0.3 p.u.

The phase deactivations (Fig. 7) evoke oscillations in the measured rotor speed and are connected with a significant increase in the measured stator current vector magnitude. These oscillations are related to the supply asymmetry that emerges from the phase deactivations. The estimated rotor speed reconstructs these oscillations, however, with low amplitude. After the deactivation of phase C, the oscillation amplitude of the measured rotor speed is

increasing and also the measured stator current magnitude oscillations. However, the drive is capable of providing a continuous operation and the desired load, paid with the increase in the stator current in the remaining phases.

Fig. 8 demonstrates the open-phase fault generation for nominal load case operation.

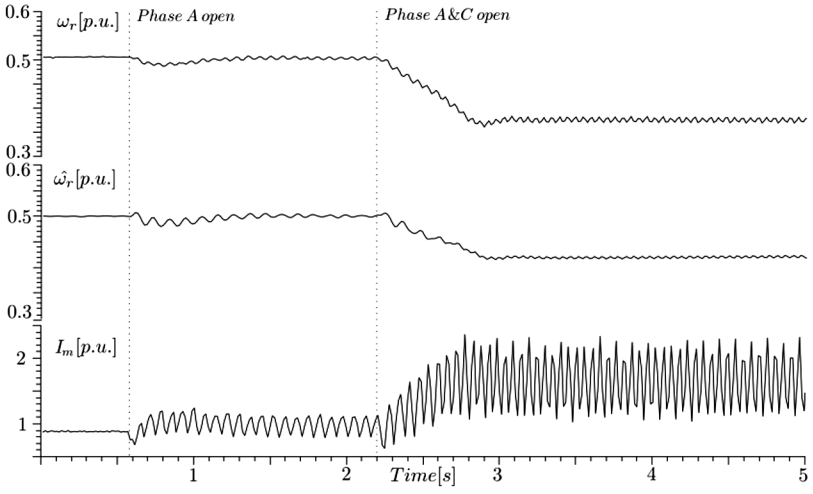

Fig. 8. Operation capabilities of the five-phase induction motor drive with one or two opened phases under nominal load.

The desired speed is decreasing due to the limitation of the control system (Fig. 8), which allows a drive operation with an average stator vector magnitude current of two times the nominal value (Fig. 4). It is apparent that the rotor speed drop can be compensated with the cost of a higher allowed current limit. Oscillations are also present in the experiment shown in Fig. 7.

The open-phase detection solutions in the study by Wilczynski et al. (2017b) demonstrated a possibility of detecting the lag of phases in an algorithm, which buffers the individual measured stator current values and concluded the lag of phases through a non-current measurement for a specific period. The presented method is based on frequency analysis of the estimated observer values.

First, Fig. 9 demonstrates the FFT (Fast Fourier Transform)(2,048 samples and 400 Hz sample frequency) of the measured stator current vector magnitude during the successive phase deactivation at a rotor speed of $\omega_r = 0.8$ p.u.

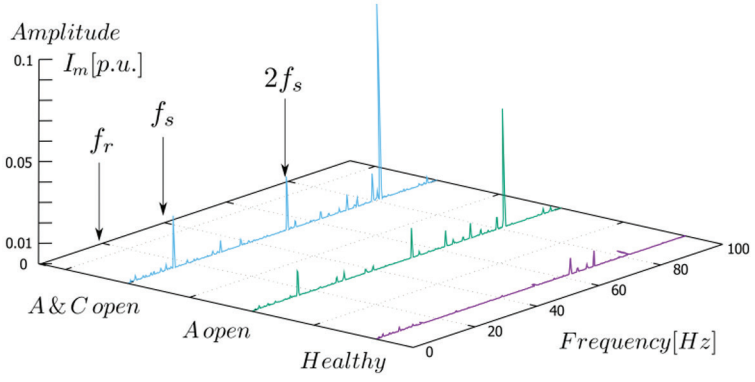

Fig. 9. Frequency analysis of measured stator current magnitude during the deactivation of phase A and phase A and C.

As can be seen in Fig. 9, the frequency analysis of the measured stator current vector magnitude presents a harmonic in the range of $2f_s$ during the deactivation of the phase and corresponds with the oscillations shown in Figs 8 and 9.

This harmonic is increasing with the deactivation of phase C. The small amplitudes (ripples) in the frequency range of 60 Hz–70 Hz can be related to possible consequences of the control system and flux synchronisation.

The reaction of the estimated rotor speed was analysed and is presented in Fig. 10.

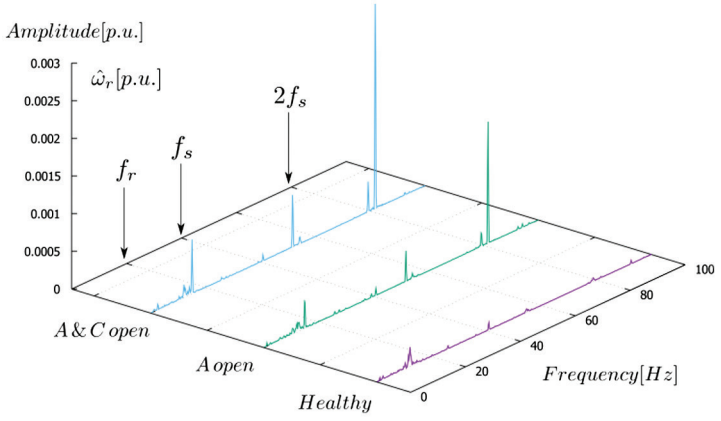

Fig. 10. Frequency analysis of estimated rotor speed estimation during the deactivation of phase A and phase A and C.

The frequency analysis (2,048 samples and 400 Hz sample frequency) of the estimated rotor speed shows only the rotor frequency during healthy operation (Fig. 10). For the case that phase A is opened, the harmonic occurs as in the previous analysis (Fig. 9) with a dominant amplitude in the frequency spectrum. If the second phase, phase C, was opened, the amplitude of the occurred harmonic increases with further opened phases. The rotor speed estimation reflects the measured stator current, however, with a more filtered spectrum.

The occurrence of this harmonic which was tested as well as in different speed ranges provides very applicable information for a fault detection method.

The application of this knowledge in a fault detection procedure was implemented in the test setup for a practical verification. An online FFT analysis of the estimated rotor speed was performed outside the control loop to save the time critical calculations for the control with a sampling period of 1.5 ms. The FFT length was limited to 256 samples to reduce the microprocessor requirements.

Fig. 11 illustrates the online frequency analysis during the closed loop operation, while a successive phase deactivation of A and C (Fig. 11a and b), and successive reactivation of phase C and A is illustrated in Fig. 12c and d. The amplitude of the highest detected harmonic $A_{\omega r}$, the frequency of the highest determined harmonic $f_{\hat{\omega}r}$, as well as the measured current of phase A, B and C is shown. The current measurements are inferior to aliasing effects, due to the long registration time, and could be only seen as rough indication, if a current lag occurs.

As can be seen in Fig. 11a and b, the control system is resistant to the phase deactivations of A and C. It is recognisable that the current in the remaining active phases is increasing with every disabled phases. Moreover, after the deactivation and the FFT calculation time, the analysis of the estimated rotor speed shows the frequency, which was in the presented case about 50 Hz between Fig. 11a and b. The deactivation of phase C (Fig. 11b) causes a further increase of the harmonics amplitude. The activation process of phase C (Fig. 11c) decreases the harmonic amplitude as well as the current in the remaining phases. The final reactivation of phase A (Fig. 11d) returns the drive operation to normal conditions and the double stator frequency harmonic disappears, which can be seen in the last stage of the experiment. The different frequency in Fig. 11d compared to Fig. 11a is related to algorithm that in this case determines the highest frequency of noise in the signal, vary permanent and is irrelevant, as can be concluded from the low amplitude share of $A_{\omega r}$.

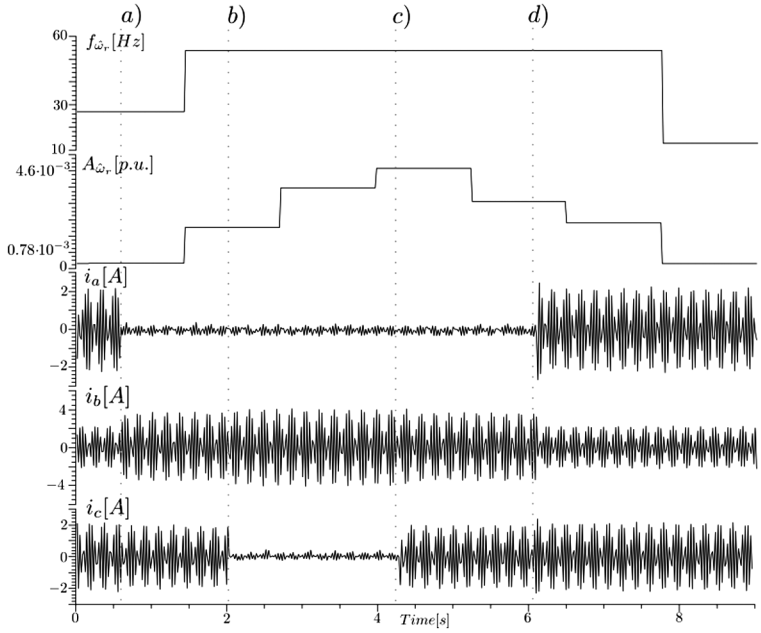

Fig. 11. Online fault detection procedure using FFT of estimated rotor speed while deactivating and reactivating phases A and C where (a) is the phase A deactivation, (b) phase A and C deactivation, (c) phase C reactivation and (d) phase A reactivation.

Despite the complexity level compared to simple open-phase detection procedures that can include the monitoring of the phase current lag, the presented procedure provides a reliable fault detection solution. The presence of the filter can cause a further current flow, if the phase fault occurs before the motor (Fig. 11). In this situation, a simple zero current detection method can lead to misinterpretations. However, the presented method will also detect this kind of fault and will not interfere with the disturbance detection method presented in the study by Strankowski et al. (2017), for the reason that unbalances of the rotor shaft are related to the rotor frequency and the additional gained knowledge can be used as enhancement of the online fault detection possibilities.

5. Conclusions

The paper presented the open-phase fault detection possibility of a sensorless five-phase induction motor drive with an LC filter and third harmonic injection. A speed observer for the first plane control system and a rotor flux observer for the second plane control system with LC filter consideration were presented to obtain the sensorless control possibility that is based only on the current sensors and the DC-link voltage sensor included in the voltage inverter.

The open-phase faults were generated with the help of circuit breakers. A continuous drive operation was possible after deactivation and reactivation of the phases. The frequency analysis of the estimated speed presented a harmonic in the range of twice of the stator frequency that occurs after the phase deactivation with dominant amplitude. This occurrence allowed an online open-phase fault detection implementation through the frequency analysis of the estimated speed. The presented procedure provided reliable fault detection during the drive operation that can be applied to five-phase induction motors.

Acknowledgments

This work was supported by the National Science Centre of Poland grant no. 2015/19/N/ST7/03078.

References

Adamowicz, M. Krzemiński, Z., Morawiec, M., Strankowski, P., Guziński, J. (2016). Sterowanie multiskalarne pięciofazową maszyną indukcyjną. *Przegląd Elektrotechniczny*, (5), pp. 108–115

Adamowicz, M., Strankowski, P., Guzinski, J. and Krzeminski, Z. (2015). Sterowanie multiskalarne pięciofazowym silnikiem indukcyjnym. In *XII Krajowa Konferencja Naukowa Sterowanie w Energoelektronice i Napędzie Elektrycznym SENE*, Łódź.

Guziński, J. (2008). Closed loop control of AC Drive with LC Filter. In *13th International Power Electronics and Motion Conference EPE-PEMC*, Poland.

Guzinski, J. (2009). Sensorless AC drive control with LC filter. In *EPE'09. 13th European Conference on Power Electronics and Applications, 2009,* pp. 1–10.

Guziński, J. (2011). *Układy napędowe z silnikami indukcyjnymi i filtrami wyjściowymi falowników: zagadnienia wybrane*. Gdańsk: Wydawnictwo Politechniki Gdańskiej.

Guzinski, J., Abu-Rub, H. and Strankowski, P. (2015). *Variable Speed AC Drives with Inverter Output Filters.* Hoboken: John Wiley & Sons.

Guzinski, J., Morawiec, M., Strankowski, P., Krzeminski, Z., Lewicki, A., Kostro, G. and Woronowski, K. (2017a). Sensorless multiscalar control of five-phase induction machine with inverter output filter. p. P.1-P.10.

Guzinski, J., Kostro, G., Strankowski, P., Morawiec, M. and Wilczyński, F. (2017b). Właściwości napędowe pięciofazowego silnika indukcyjnego klatkowego. *Automatyka Elektryka Zakłócenia*, no. Innowacje, pomiary i bezpieczeństwo w elektroenergetyce, pp. 14–26

Krzemiński, Z. (2000). Sensorless control of the induction motor based on new observer. In *International Conference on Power Electronics, Intelligent Motions and Power Quality PCIM'00*, Germany.

Levi, E. (2008). Multiphase electric machines for variable-speed applications. *IEEE Transactions on Industrial Electronics*, 55(5), pp. 1893–1909.

Levi, E., Bojoi, R., Profumo, F., Toliyat, H. A. and Williamson, S. (2007). Multiphase induction motor drives - a technology status review. *IET Electric Power Applications*, 1(4), p. 489.

Lewicki, A., Guziński, J., Strankowski, P. (2016a). Metoda wektorowej modulacji szerokości impulsów pięciofazowego falownika napięcia. *Przegląd Elektrotechniczny*, (5), pp.28–35.

Lewicki, A., Guziński, J. and Strankowski, P. (2016b). Pulse width modulation method for a five phase voltage source inverter. *Electronics Review*, 1(5), pp. 28–35

Lewicki, A., Strankowski, P., Morawiec, M. and Guzinski, J. (2017a). Strategia wektorowej modulacji szerokości impulsów dla wielofazowych falowników napięcia. In *XIII Krajowa Konferencja Naukowa Sterowanie w Energoelektronice i Napędzie ElektrycznymSENE 2017*

Lewicki, A., Strankowski, P., Morawiec, M. and Guziński, J. (2017b). Optimized space vector modulation strategy for five phase voltage source inverter with third harmonic injection. In *Power Electronics and Applications (EPE'17 ECCE Europe), 2017*, p. P–1.

Lewicki, A., Strankowski, P., Morawiec, M. and Guziński, J. (2017c). Generating the output voltages in the 5-phase voltage source inverters. *Automatyka Elektryka Zakłócenia*, pp. 28–37

Payami, S. and Behera, R. K. (2017). An improved DTC technique for low-speed operation of a five-phase induction motor. *IEEE Transactions on Industrial Electronics*, pp. 3513–3523.

Strankowski, P., Guziński, J., Morawiec, M., Lewicki, A. and Wilczynski, F. (2017). Sensorless disturbance detection for five phase induction motor with third harmonic injection. *11th IEEE International Conference on (CPE-POWERENG)*, 2017, pp. 387–391.

Ward, E. E. and Härer, H. (1969). Preliminary investigation of an inverter-fed 5-phase induction motor. *Proceedings of the Institution of Electrical Engineers*, pp. 980–984.

Wilczynski, F., Morawiec, M., Strankowski, P., Guziński, J. and Lewicki, A. (2017a). Sensorless field oriented control of five phase induction motor with third harmonic injection. In *Compatibility, Power Electronics and Power Engineering (CPE-POWERENG),11th IEEE International Conference on*, 2017, pp. 392–397.

Wilczynski, F., Strankowski, P., Guzinski, J., Morawiec, M., Lewicki, A. and Kostro, G. (2017b). Działanie napędu z pięciofazowym silnikiem indukcyjnym przy uszkodzeniu faz stojana. *Autom Elektr Zakłócenia*, 8, pp. 28–37.

Wilczynski, F., Strankowski, P., Guzinski, J., Morawiec, M. and Lewicki, A. (2017c). Vector control of five phase induction rotor with rotor flux shape optimization - Sterowanie wektorowe pięciofazowym silnikiem indukcyjnym z optymalizacją rozkładu strumienia wirnika. *Wiadomosci Elektrotechniczne*, pp. 23–28.